

A Low-Cost Compact Metric Adaptive Optics System

Justin D. Mansell¹, Brian Henderson, Brennen Wiesner, Robert Praus, and Steve Coy
Active Optical Systems, LLC, 2021 Girard Ste 150, Albuquerque, NM 87106

ABSTRACT

The application of adaptive optics has been hindered by the cost, size, and complexity of the systems. We describe here progress we have made toward creating low-cost compact turn-key adaptive optics systems. We describe our new low-cost deformable mirror technology developed using polymer membranes, the associated USB interface drive electronics, and different ways that this technology can be configured into a low-cost compact adaptive optics system. We also present results of a parametric study of the stochastic parallel gradient descent (SPGD) control algorithm.

Keywords: Low-cost, inexpensive, compact, adaptive optics, polymer deformable mirror, metric adaptive optics, wavefront sensorless adaptive optics, stochastic parallel gradient descent, SPGD.

1. INTRODUCTION

For the first few decades of adaptive optics, the specialized equipment required to complete a system was too expensive for wide-spread commercial adoption. In recent years, researchers and product engineers have worked to reduce the cost of every part of adaptive optics systems in an attempt to address commercial needs. Electrostatic deformable mirrors have been created using mass-fabrication compatible technology like MEMS.^{1,2,3,4} Wavefront sensors have been created using high-speed CMOS imaging technology.⁵ Algorithms like stochastic parallel gradient descent (SPGD)⁶ and Zernike optimization⁷ were developed and demonstrated to use even lower-cost higher speed feedback, such as photodiodes. Advances in integrated circuit technology have created tiny microprocessors powerful enough for adaptive optics and cheap enough to be in toys and appliances.⁸ Finally, investment in telecommunications has enabled the development of relatively low-cost drive electronics to interface digital signals to electrostatically actuated deformable mirrors.

All of this development has enabled researchers to begin to create low-cost adaptive optics (AO) systems. In 2000, Patterson *et al.* used a membrane deformable mirror to create a low-cost AO system with an estimated production cost of \$25,000.⁹ This corresponds to \$30,250 in today's dollars.¹⁰ We have worked to develop products that further reduce the cost of adaptive optics systems. In this paper we present some of these developments. We also describe and characterize a low-cost adaptive optics system that we sell for \$7,500, more than 4 times less expensive than the system described by Patterson.

2. APPLICATIONS OF ADAPTIVE OPTICS

Virtually any optical system today that is deleteriously affected by aberrations can be improved with adaptive optics. Unfortunately for those of us creating these systems, it is not always advisable to add adaptive optics. We believe that the primary barriers to adoption for AO are cost, inertia, and complexity, with the biggest of these being cost. Inertia refers to the applications that already are employing another technique for removing system distortions. For example, some laser applications use a pinhole at the focus of the beam to filter out the aberrated light. If the aberrations are not too severe, the power reduction in the beam will be minimal and the technique works well. It's hard to compete with an effective low-cost solution like this, but even if we could compete with this on cost, complexity often becomes the next barrier. Almost everyone trained in optics understands how a pinhole can filter a beam, but very few have been trained in how to make an adaptive optics system work. Product developers see the implementation of adaptive optics as a huge investment that may not translate into a more competitive product.

¹ jmansell@mza.com; phone 1 505 245-9970 x122

One goal of this community of late has been to try to address these key barriers to get product developers to consider adaptive optics. Several significant applications are currently actively evaluating adaptive optics including (in no particular order) laser machining, photolithography, astronomy, microscopy, free-space laser communications, and directed energy weapons. We present here a description of our first low-cost AO product that will be good for some of these applications.

3. POLYMER MEMBRANE DEFORMABLE MIRRORS

The most unique item to an adaptive optics system is the deformable mirror. Other than adaptive optics, there is virtually no other application that uses deformable mirrors, which makes it one of the most costly items in the system because it cannot directly leverage any existing investment. The development of MEMS deformable mirrors enabled researchers to tap into a mass-fabrication compatible way of creating these devices that has been heavily supported by the integrated circuit industry.

MEMS fabrication has its drawbacks though. MEMS fabrication can be inexpensive when the number of devices being created is very large. The exact break point is a matter of great debate and depends on many factors, but it is probably greater than 1,000 units and may be as large as 100,000 units depending on the application and the required setup costs. In this early phase of adaptive optics adoption, it is difficult to amortize these start-up costs. Foundry fabrication has been effective for many types of devices, but most devices created in a foundry require some post processing, usually to increase the surface quality. There are some specifications that MEMS deformable mirrors will probably never be able to meet. For example, devices that need to be very large, very high surface quality, and/or have high laser power handling are difficult to create using conventional MEMS technology.

In considering these drawbacks of MEMS, we decided to investigate optical polymer membrane deformable mirrors. One of the first membrane deformable mirrors was described in 1977 by Grosso and Yellin.¹¹ They created a deformable mirror comprised of a metal membrane suspended over an array of electrostatic electrodes. In 1993, Miller *et al.* described a micromachined device membrane deformable mirror.² This architecture was subsequently commercialized by Vdovin.³

In 1994, Takami *et al.* described using a similar architecture, but replaced the metal membrane with a nitrocellulose pellicle.¹² Pellicles had been developed by the integrated circuit industry in the decade before this to protect the surfaces of photolithographic masks from contamination and damage during use.¹³ During the 1980's, use of pellicles became an industry standard. These pellicles are created with great optical quality to avoid distortion of the printed patterns and with enough durability to withstand everyday use, but with sufficiently low cost to be effectively disposable. The optics industry uses pellicles routinely to sample beams with significant wavefront curvature without inducing distortion. There are many companies world-wide that make optical pellicles. Optical pellicles offer greater flexibility than the MEMS deformable mirrors because they can be easily manufactured from the constituent parts upon demand to have varying tension, thus giving the designer control over the trade-off between resonance frequency and throw.

The deformable mirror described by Takami used a MACOR substrate to create the electrodes. MACOR is a machinable glass ceramic that can be polished and coated with copper to create the electrodes. Unfortunately MACOR is not widely available and is expensive. We decided to replace the expensive MACOR with more conventional FR4 printed circuit board material that is widely used by the electronics industry. This architecture allows us to not only create a low-cost deformable mirror, but also one that does not depend on the expensive infrastructure required for MEMS and is scalable to mass fabrication.

3.1 The AOS Polymer Membrane Deformable Mirror Device

Figure 1 shows our pellicle membrane deformable mirror device and its corresponding package. The device shown is a 1" diameter pellicle with a 1 3/8" outer diameter aluminum frame. Electrically, each actuator on the deformable mirror acts like a small capacitor. The capacitance of each actuator depends on the geometry, but is typically ~1 nF. The mirror surface itself is usually statically aberrated in an astigmatic term that is $\sim\lambda/2$ per inch. Since the mirror surface is mounted to a thick stiff aluminum frame, the mirror surface figure typically exceeds its MEMS membrane mirror counterparts. Although for most visible light applications it is not necessary, the mirror surface can be coated with a high reflectivity multi-layer dielectric coating for laser operation.

The package was created using a commercial die-cast aluminum package 2.4" x 4.4" x 2". The front of the package was machined to accept an adapter for the ThorLabs SM1 beam tube components. This enables the placement of a window on the device to protect the mirror surface or a cap to seal the package when not in use. This window can be replaced with a lens or lens system as well to compensate the parabolic bias of the deformable mirror. The back of the package was machined to allow it to be attached to a ThorLabs 2" kinematic platform mount. The one-inch diameter DM comes in three different actuator patterns: 25-actuator segmented annular, 31-actuator hexagonal grid, and 32-actuator square. Any of the three one-inch diameter deformable mirrors sells for \$1,500.

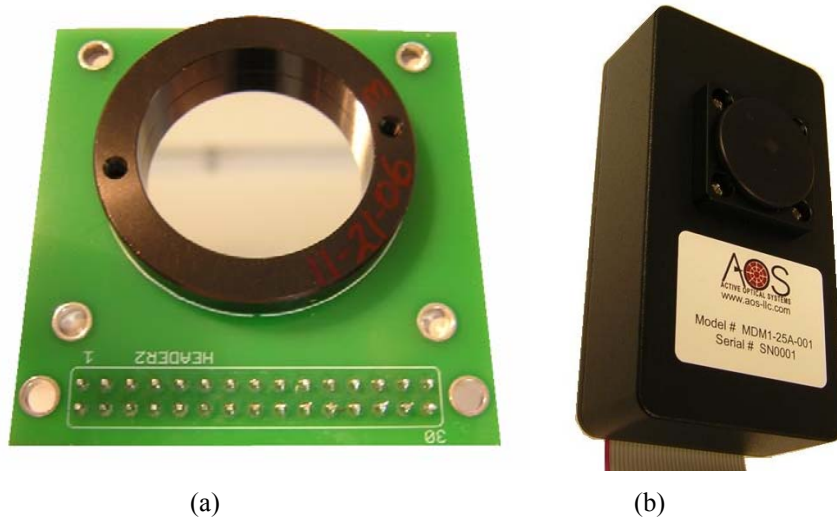


Figure 1 - (a) A membrane deformable mirror comprised of an aluminum coated optical pellicle and a conventional FR4 printed circuit board with a 0.1" spacing ribbon cable header. (b) shows a packaged deformable mirror capable of being mounted to a standard 2" ThorLabs kinematic platform mount.

To characterize the maximum throw of our device, we performed an experiment where the pellicle was mounted in a kinematic optic mount and a silicon wafer was used as a uniform electrode mounted to a translation stage. We translated the silicon wafer towards the pellicle under a fixed bias of 330V and monitored the focal length of a collimated beam reflected from the pellicle. We found that the pellicle mirror surface underwent snap-down (a runaway effect where the parabolic electrostatic force exceeds the linear mechanical restoring force in the membrane causing a rapid acceleration of the membrane towards the surface that usually results in a spark discharge between the membrane and the electrodes) when the focal length was ~ 1 m or the throw was about 40 microns in focus (~ 80 microns of OPD). Unlike its MEMS counterparts, the mirror membrane did not rupture despite being snapped down electrostatically hundreds of times during the execution of this experiment. The only apparent damage to the membrane surface was the sputtering of the thin aluminum layer from the back surface of the pellicle.

We used a similar setup to characterize the resonant frequency of the polymer membrane deformable mirror. A collimated beam of light was reflected from the surface of the mirror and then focused onto the edge of a small photodiode. The potential difference between the mirror and the large silicon wafer electrode was then varied to cause the focus to move along the optical axis, which created a varying intensity on the photodiode. We first measured the amplitude of the mirror's response on the photodiode to a fixed sinusoidal frequency. We found a clear peak in the resonance around 550 Hz. We also measured the step response of the mirror by driving the DM with a slow square-wave signal. Analysis of the photodiode signal showed the expected decaying oscillation at the same frequency. Although this resonance frequency is too low for some of the hardest problems in adaptive optics, it is sufficient for many of them. The manufacturer of this pellicle has measured the resonance of some of the pellicle products near 3 kHz when special care is taken to increase the tension during the manufacture.

3.2 Operation of a Membrane Deformable Mirror Relative to a Plate-Type Deformable Mirror

Membrane deformable mirrors are significantly different than conventional plate-type deformable mirrors, so some description of their key differences is warranted. The influence function of a membrane DM, which is the shape of the mirror surface obtains in response to actuation of a single actuator, is different than the plate-type DM in that it is not very localized, but instead extends to the edge of the mirror surface. Since voltage-controlled electrostatic forces can only pull on the mirror membrane, the DM needs to be operated about a bias. Unlike a plate-type DM, the bias term of a membrane DM is not a piston, but is parabolic because the edges of the mirror membrane are fixed. This can usually be easily compensated optically by defocusing a telescope or moving the focal plane of the imaging system. Finally, the voltage response is parabolic without hysteresis, which is typically much easier to use than the hysteretic non-linear response of the PMN or PZT actuators used in a plate-type DM.

4. DRIVE ELECTRONICS

The next most specialized component of the adaptive optics system is the drive electronics that interface the control computer to the deformable mirror. The goal behind this design was to create an electronics package that was efficient, compact, and low-cost. In designing the drive electronics, we started with a commercially available 32-channel high voltage amplifier chip designed for driving electrostatic actuators like those in MEMS. We created analog signals for this amplifier chip using COTS high-speed 8-bit digital to analog converters (DACs). A \$7 microcontroller was used to provide a full-speed USB interface from the control computer to the DACs. The printed circuit board that marries all of these parts together into a drive electronics board is only 4" x 3.2" on a side. Although each board is only capable of writing to 32 channels, we designed a digital port for cascading multiple boards together and addressing more channels.

We combined that with a power supply and power conditioning board into a convenient metal box that is only 6" x 6" x 3" and runs from wall-plug power. Figure 2 shows the resulting product. In addition to the USB interface on the front panel, there is a 37-pin D-sub female connector for the DM connection that provides an interface that is safe from accidental contact and polarized to avoid connection ambiguity that can be a problem in ribbon cable header connections.



Figure 2 - AOS's deformable mirror drive electronics package

The full-speed USB bus updates at 1 kHz, so that is the maximum frequency the interface will support. We measured the write time of 32 channels to be ~550 μ s. The maximum output voltage is 295 V.

The firmware is designed to take a single 8-bit character command from the user and then a series of parameters to that command based on the command. For example, “R” resets all the channels to zero with no further parameters. The command “A” sets all the channels to a voltage using a single character voltage level as the only parameter. Some commands send data back to the control computer as well. For example, “P” returns the photodiode voltage as an 8-bit number corresponding to a 0 to 5V input. A one second timer was implemented for the completion of a command to avoid requiring a hardware reset in the case of an interrupted command. We also implemented code to enable new firmware to be loaded by the user via the USB port.

During the development of the drive electronics, we began to realize the tremendous computational power in the microcontroller we were using to provide a simple USB interface to the PC and re-designed the drive electronics to allow the microcontroller to get feedback. We modified the drive electronics board to include an optional trans-impedance amplifier and an interface to the microcontroller’s on-chip 10-bit analog to digital converter (ADC), of which we typically only used the most significant 8 bits. The microcontroller firmware was also modified to implement a version of the SPGD optimization algorithm, which is described in detail later in this paper.

5. ADAPTIVE OPTICS SYSTEM

5.1 Experimental Setup

Figure 3 shows the optical setup we used to demonstrate the optimization capability of our drive electronics. Light from an unpolarized 633nm helium-neon laser is expanded with a telescope comprised of a 12-mm focal length lens (L1) and a 500-mm focal length lens (L2) to a 25 mm diameter beam. A 12-mm diameter iris (A1) placed inside the telescope was used to control the size of the beam illuminating the DM. After being expanded, the light illuminated a beam splitter (BS1) with a portion of the light going to a reference flat (M1) and the remainder to a 25-mm diameter membrane deformable mirror (DM). Then the light is combined on the beam splitter and sent through a 250-mm focal length 50-mm diameter lens (L3) to a focus on an aperture (A2) in front of a photodiode (PD). When the photodiode was replaced by a camera, the setup could be used as an interferometer. When the reference flat (M1) is blocked, the system can be used to perform metric adaptive optics. An additional camera was used to capture far-field images by splitting the beam (BS2) after L3 and sending that light to a camera that imaged the focus with a 4-mm focal length lens to get a good point-spread function measurement.

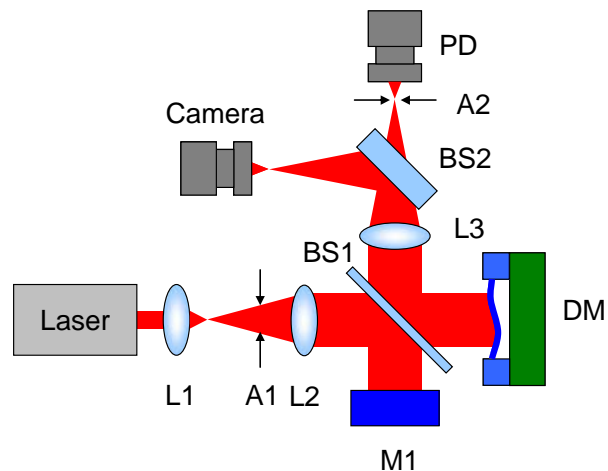


Figure 3 - Optical setup used in the adaptive optics experiment.

When the photodiode was replaced by a camera, the setup could be used as an interferometer. When the reference flat (M1) is blocked, the system can be used to perform metric adaptive optics. An additional camera was used to capture far-field images by splitting the beam (BS2) after L3 and sending that light to a camera that imaged the focus with a 4-mm focal length lens to get a good point-spread function measurement.

We used two different kinds of apertures in front of the photodiode in this experimental setup. In one configuration, we used a 12-mm diameter zero-aperture iris that allowed us to vary the aperture size. In a second configuration we used a 20-micron diameter pinhole in front of the photodiode. Both the iris and the pinhole were placed in the beam along the optical axis to maximize the power through them for a bias voltage on the DM of about 120 counts. Since the DM has a parabolic voltage dependence, this would normally be set to $255/\sqrt{2}$, which is ~ 180 counts, but this DM had such a large throw it was unnecessary to use this much of the range of the drive electronics for the bias condition. The photodiode was connected to the BNC input of the drive electronics and to a USB-interface digitizing oscilloscope for independent monitoring of the system efficacy.

The aberration in this optical system had several different sources. The DM had about $\frac{1}{2}$ of a wave of astigmatism in its uncorrected state. The optical system was not perfectly aligned, which induced some aberrations. The beam splitter that sampled light for the PSF diagnostic camera was not a pellicle, but was a 50-mm diameter plate about 6 mm thick, which caused further aberration.

5.2 Optimization & Control Algorithms

Stochastic Parallel Gradient Descent

We implemented a simple version of stochastic parallel gradient descent (SPGD) in the microcontroller firmware to enable the drive electronics to do complete closed-loop adaptive optics control without the need of an external control computer. The AO system is currently being commanded into operation via the USB interface, but it is possible to enable the controller to boot into this mode without any external computer at all.

The algorithm behavior is typical for two-step SPGD. In the first step, the microcontroller evaluates the current position of the mirror and generates a vector direction for the next step which is applied to the current position. The new vector is generated as follows:

$$V' = V + dV$$

where $dV = \Delta \bullet \text{rand}(N)$,
 Δ is the maximum step size,
 $\text{rand}(\dots)$ is a random number vector from -1 to +1, and
 N is the number of actuators

Then the computer waits a user-specified delay time to allow the electronics and mirror to settle into position and evaluates the step position. From the measurement of the previous position and the change in the metric function, M , the new position is calculated as

$$V' = V + \eta(M_{\text{initial}} - M_{\text{step}})dV,$$

where η is the gain factor. In the PC implementation of this algorithm, we kept track of the best result and returned to that result after each iteration, but on the microcontroller the tracking of the best position was not done.

Modified Dithering (Single-Axis Brute Force Searching)

We also explored a simplified dithering algorithm for comparison. In this algorithm, each actuator is scanned over its full range with small steps while the metric is evaluated. This algorithm was chosen over traditional dithering because the aberration was static and it was thought to be more robust to local minima. The actuator command with the largest metric value is then kept and the next axis is scanned. This algorithm can be repeated after scanning through the entire actuator set for better performance.

5.3 PC Implemented Optimization

We implemented each of the two algorithms described above on a PC to quickly explore the efficacy of the optimization algorithms. The optimization functionality was added to our existing C# drive electronics control software. Figure 4 shows the simple user interface we used to evaluate the optimization algorithms. The “Optimization” group box houses all the controls of the optimization. The “PD” button allows the user to read from the photodiode. The “Optimize” button runs the SPGD optimization routine using the parameters below. The “Brute” button runs the brute force algorithm with the delta control being used for the step size and the iteration control being used for the number of times the algorithm repeats scanning all the actuators.

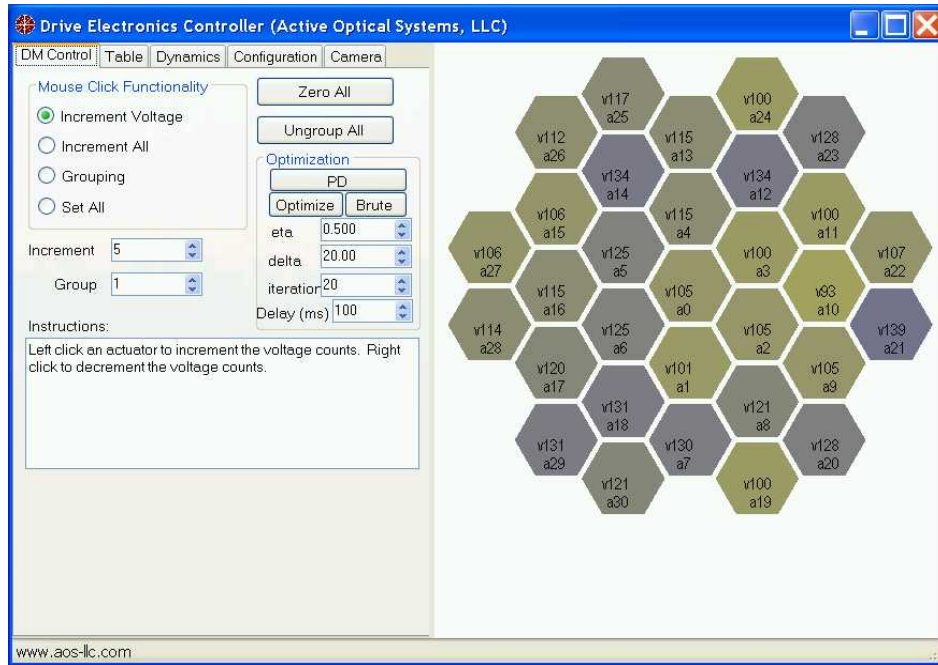


Figure 4 - Simple GUI added to the existing drive electronics for exploring optimization.

We initially evaluated both algorithms with the iris aperture in front of the photodiode, but moved to the 20-micron pinhole for more accurate feedback. The beam incident on the DM in these experiments was 25-mm in diameter. In every study, the mirror was biased in curvature to the position that maximized the photodiode output voltage before beginning optimization.

Figure 6 shows the results of two iterations of the dithering algorithm. In these two iterations, ~8,000 metric evaluations were performed. The photodiode signal increased from around 48 counts, where the mirror was in the optimal bias condition, to 256 counts at the end of the search.

Figure 5 shows the results of 300 iterations (600 metric evaluations) of the SPGD algorithm. The SPGD algorithm did not produce as high a photodiode signal, but the far-field pattern evaluated on the metric camera was good. This

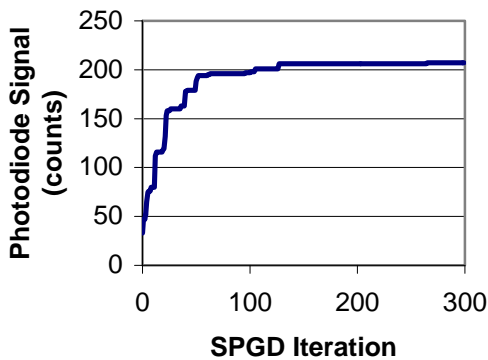


Figure 5 - Results of the SPGD Optimization

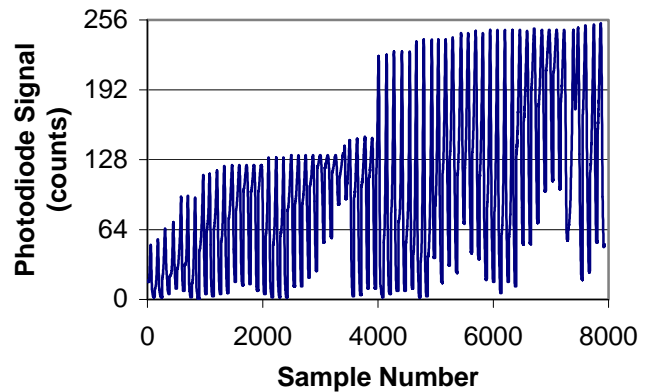


Figure 6 - Results of the Brute Force Search

algorithm was significantly faster than the simple dithering algorithm, so it was chosen for implementation on the microcontroller.

Figure 7 shows the focal spot images captured from one of the AO runs. The DM and the optical system are responsible for the aberrations on the beam resulting in the distorted spot. The high spatial frequency ripple on the images is caused by the cover glass on the CMOS imager.

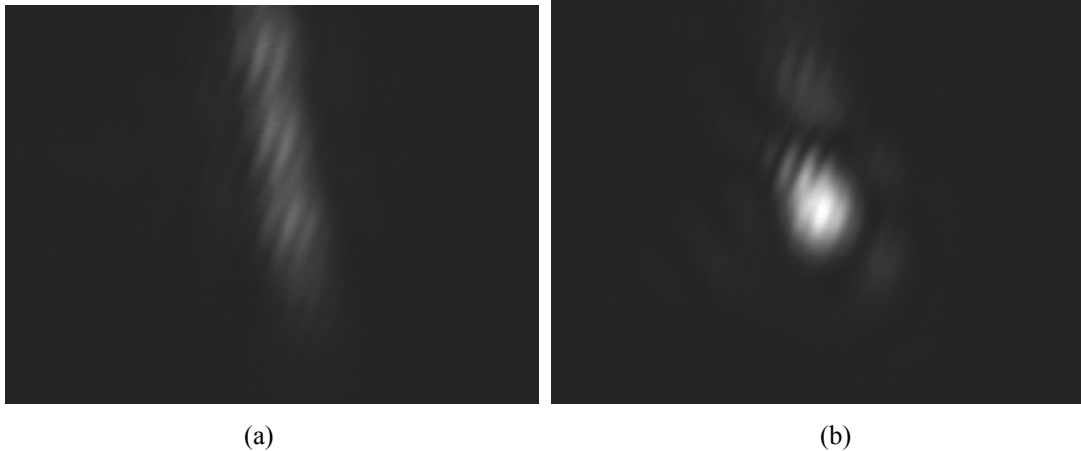


Figure 7 - Focused spot without (a) and with (b) the AO loop closed.

5.4 Microcontroller SPGD

Once the SPGD algorithm was tested on our PC platform, it was added to the microcontroller firmware. For simplicity and flexibility, we used the USB interface to command the microcontroller, but it is trivial to have this algorithm execute upon power-up. The command to start the optimization using SPGD that was added to the firmware has the following format:

O[eta][delta][delay][iterations byte 1][iterations byte 2]

where eta is the one-byte SPGD gain factor, which was implemented as the byte – 100 then difference divided by 100 to achieve values less than 1.0 and to add the capability of changing the sign of the gain, delta is the magnitude of the step in DAC counts, delay is the time to wait between applying voltages and measuring the metric input in milliseconds, and the product of the two iterations bytes is the number of iterations to perform before stopping the optimization.

The Effect of the SPGD Tuning Parameters

The microcontroller implementation of the SPGD algorithm was substantially faster than the PC implementation because it did not rely on the USB interface for commands and feedback. This enabled us to perform a rapid parametric study of the SPGD algorithm. We did the following experimentation with the iris aperture in metric AO configuration and the beam at 25-mm diameter using an iris instead of a pinhole. The set of figures in Appendix A shows the result of averaging 20 different realizations while scanning over 5 different values of delta and 5 different values of eta using a 30 ms delay between writing voltages to the DM and reading the photodiode to ensure that the DM had stabilized. We later found that this delay was excessive, but it eliminated any possibility of insufficient delay.

The average data was analyzed for three different characterization parameters: 10% to 90% rise time, final converged value averaged over the last 100 valid samples, and ripple determined from the 90% rise point to the end of the valid data. Figure 9 shows the results of this data reduction. The results generally show that as the gain (η) or the step size (Δ) increases, the final value decreases, the converged rms decreases, and the rise time decreases. There does appear to be an optimum range of values for the highest final value for this configuration around a gain of 0.15 and a range of counts from 5 to 8. Essentially, adjustments that make the system faster generally serve to reduce the converged final value and increase the converged rms noise.

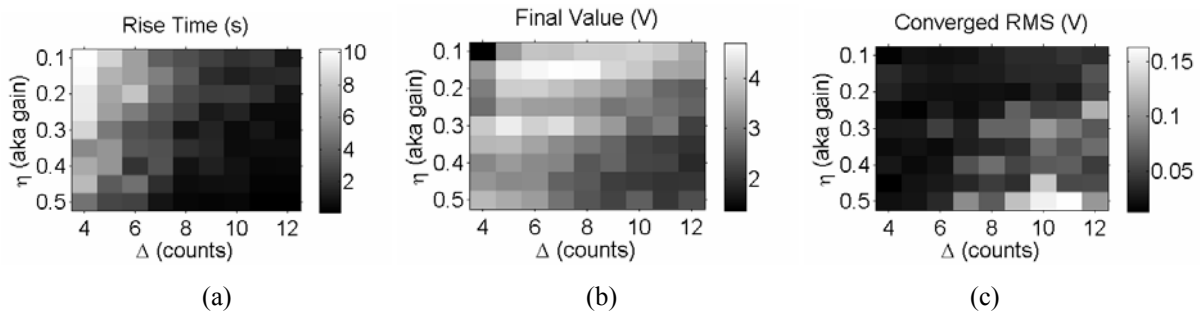


Figure 9 - Rise time (a), converged final value (b), and converged RMS (c) for the microcontroller SPGD algorithm.

The effect of delay time was evaluated for one of the best parametric values where $\eta = 0.2$ and $\Delta = 4.0$. Figure 8 shows the results of this scan where each trace is the average of 10 different runs. This result confirms that the 30 ms delay used earlier was sufficient. It also shows that 18 ms of delay is sufficient to achieve the best possible final converged value.

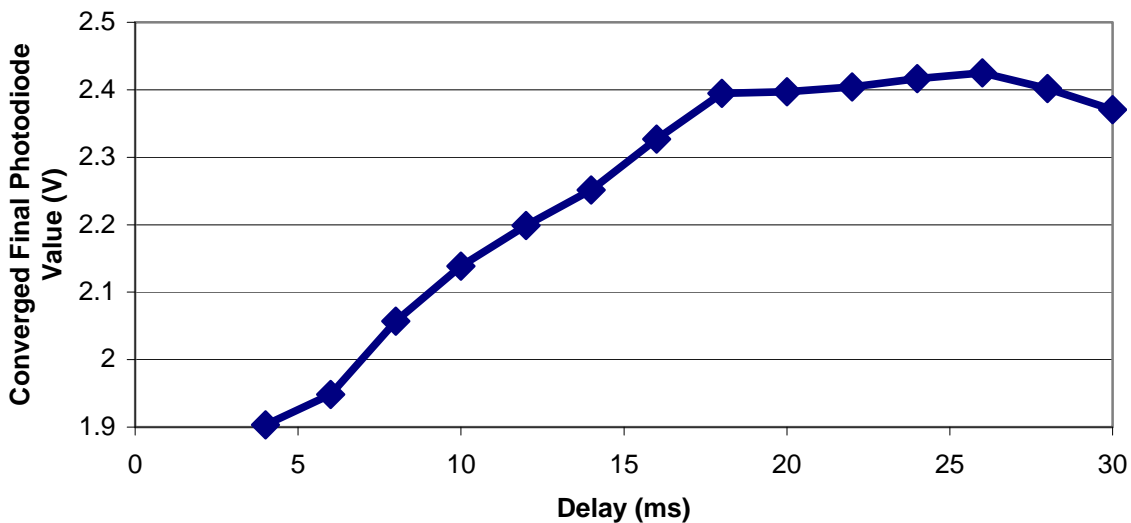
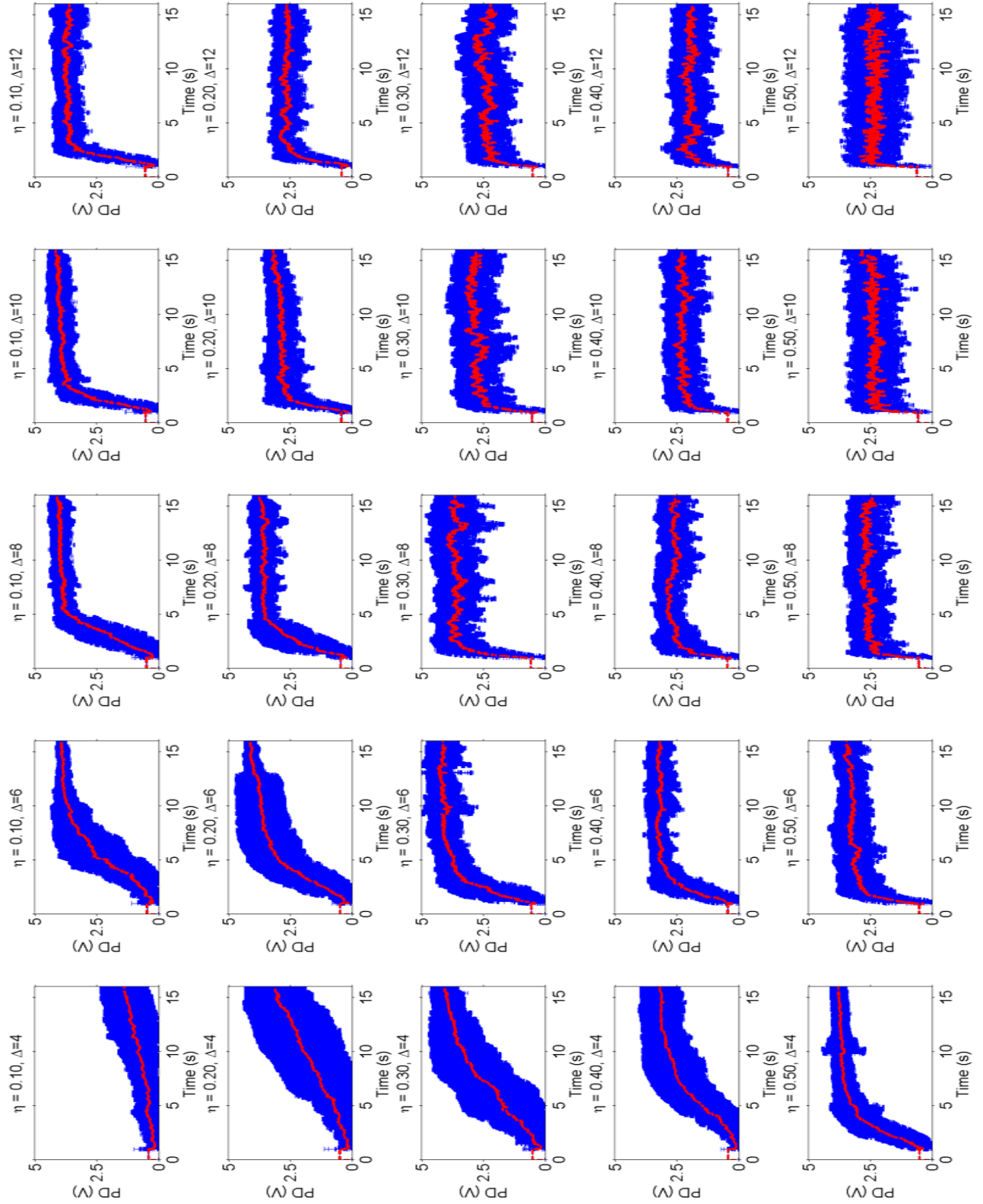


Figure 8 - Final converged value with respect to the delay between the voltage actuation and the photodiode read.

6. CONCLUSIONS

We have described a new kind of polymer membrane deformable mirror, drive electronics, and a low-cost adaptive optics system that is commercially available for \$7,500. From the parameter exploration of the SPGD algorithm on the microcontroller, we have determined the effect of the gain (η) and step size (Δ) on the system performance. We have also explored the effect of reducing the delay between writing the voltage to the DM and sampling the photodiode. In the future, we will continue to work on the component technologies to further reduce this cost. We are also working on developing a low-cost adaptive system with wavefront sensor feedback.

Appendix A: Average (red) and standard deviation (blue) photodiode data from 20 different realizations of the microcontroller SPGD algorithm with a 30ms sampling delay while varying the gain (η) and the step size (Δ).



REFERENCES

-
- ¹ J.D. Mansell and R. L. Byer, "Micromachined silicon deformable mirror", SPIE Proc. Vol. 3353, (1998).
- ² L.M. Miller, M.L. Argonin, R.K. Bartman, W.J. Kaiser, T.W. Kenny, R.L. Norton, E.C. Vote. "Fabrication and characterization of a micromachined deformable mirror for adaptive optics applications", SPIE Vol. 1945, 421-430 (1993).
- ³ G. Vdovin and P. M. Sarro. "Flexible mirror micromachined in silicon", Applied Optics 34, 2968-72 (1995).
- ⁴ T. Bifano, J. Perreault, and P. Bierden. "A micromachined deformable mirror for optical wavefront compensation", SPIE Vol. 4124, 7-14 (2000).
- ⁵ J. D. Mansell, P. B. Catrysse, E. K. Gustafson, and R. L. Byer. "Silicon Deformable Mirrors and CMOS-based Wavefront Sensors", SPIE Vol. 4124, 15-25 (2000).
- ⁶ M. A. Vorontsov, "Decoupled stochastic parallel gradient descent optimization for adaptive optics: integrated approach for wave-front sensor information fusion," J. Opt. Soc. Am. A **19**, 356-368 (2002).
- ⁷ M. J. Booth, "Wavefront sensorless adaptive optics for large aberrations," Opt. Lett. **32**, 5-7 (2007).
- ⁸ http://www.microchip.com/stellent/groups/designcenter_sg/documents/designcenter/en500059.pdf
- ⁹ C. Paterson, I. Munro, and J. Dainty, "A low cost adaptive optics system using a membrane mirror," Opt. Express **6**, 175-185 (2000).
- ¹⁰ <http://www.bls.gov/cpi/>
- ¹¹ R. P. Grosso and M. Yellin, "The membrane mirror as an adaptive optical element", J. Opt. Soc. Am., **67**, 399-406, (1977).
- ¹² H. Takami et al., "Membrane deformable mirror for SUBARU adaptive optics", SPIE Proc. 2201-78, 762-7 (1994).
- ¹³ S. Wolf and R. N. Tauber, *Silicon Processing for the VLSI Era, Volume 1-Process Technology*, 486-89, Lattice Press, Sunset Beach, CA (1986).